Electronic Supplementary Material (ESI) for Polymer Chemistry.

Supporting information

RAFT/ROP binary polymerization towards well-defined graft copolymers

Shuang Zhang,[#a] Ning Ren,[#b] Xiaoyu Li,[a] Yan Xiao,[*a] Meidong Lang[*a] and Xinyuan Zhu[*b]

[a] Shanghai Key Laboratory of Advanced Polymeric Materials, Key Laboratory for Ultrafine Materials of Ministry of Education, School of Materials Science and Engineering, East China University of Science and Technology, 130 Meilong Road, Shanghai 200237, China.

[b] Frontiers Science Center for Transformative Molecules, School of Chemistry and Chemical Engineering, Shanghai Jiao Tong University, 800 Dongchuan Road, Shanghai 200240, China.

[*] Corresponding to Yan Xiao (yxiao@ecust.edu.cn), Meidong Lang (mdlang@ecust.edu.cn) or Xinyuan Zhu (xyzhu@sjtu.edu.cn).

[#] These authors contributed equally to this work.

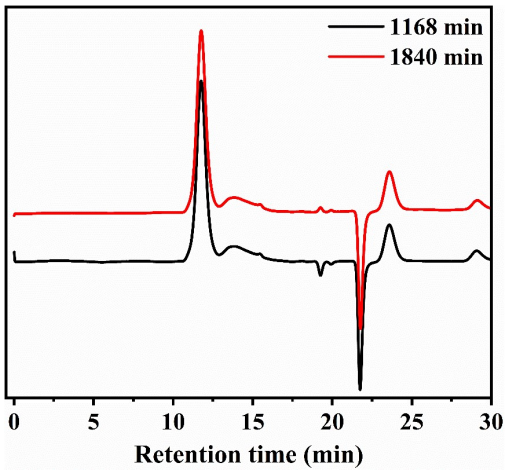

Fig. S1 GPC traces of PHEAA-*g*-PCL synthesized by RAFT/ROP binary polymerization after extending the reaction time.

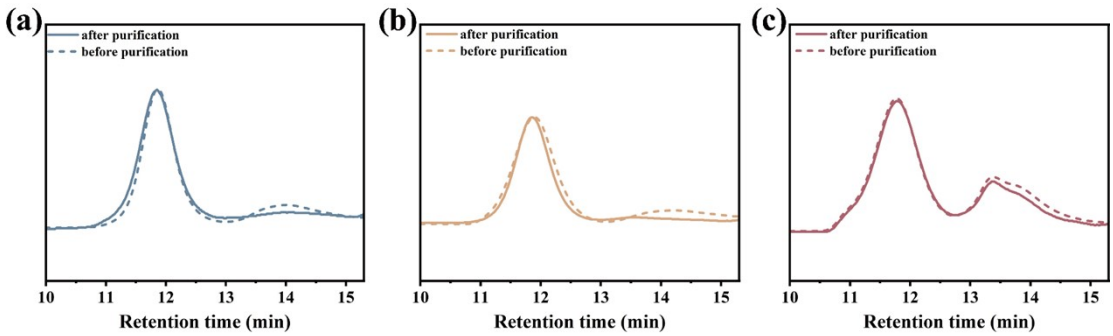

Fig. S2 GPC traces of $PHEAA_{50}$-*g*-PCL_{20} synthesized by (a) RAFT/ROP binary polymerization; (b) "grafting-through"; (c) "grafting-from".

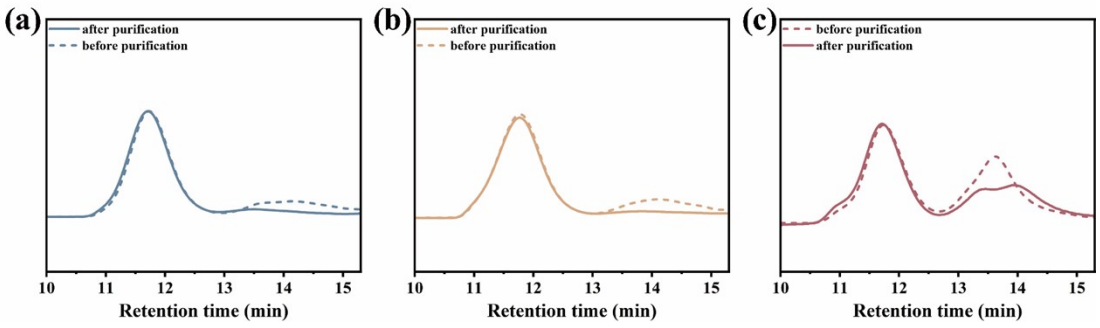

Fig. S3 GPC traces of $PHEAA_{100}$-*g*-PCL_{20} synthesized by (a) RAFT/ROP binary polymerization; (b) "grafting-through"; (c) "grafting-from".

Table S1 Summary of graft copolymers $PHEAA_{100}$-*g*-PCL_{20} prepared via three methods.

Entry	Synthesis method	Time (h)	Conversion (%)[a]		$M_{n,GPC}$[b] (Da)	PDI[b,c]
			HEAA	CL		
1	RAFT/ROP binary polymerization	24	89	82	93900	1.10
2	grafting-through	48	90	94	90700	1.11
3	grafting-from	48	85	93	97500	1.23

[a] Calculated from the integration ratios of the characteristic peaks ^{1}H NMR.

[b] Determined by GPC eluted with DMF calibrated by PMMA standards.

[c] Integration of PDI does not include the peak at higher elution times.

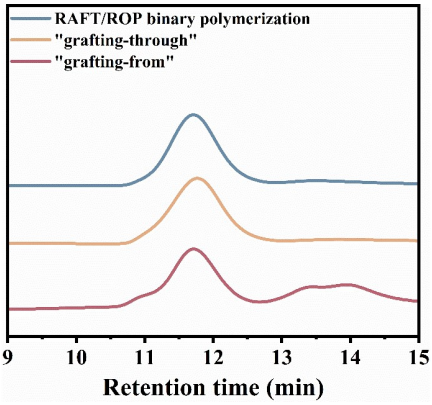

Fig. S4 GPC traces of purified $PHEAA_{100}$-*g*-PCL_{20} synthesized by (a) RAFT/ROP binary polymerization; (b) "grafting-through"; (c) "grafting-from".

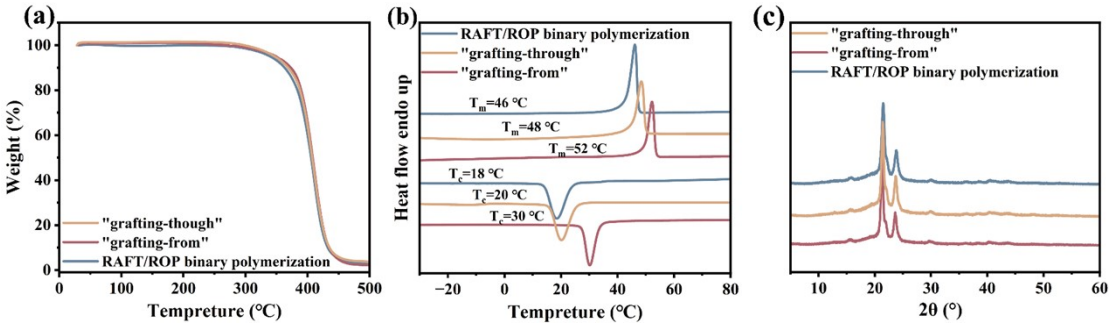

Fig. S5 Performance characterization of $PHEAA_{100}$-*g*-PCL_{20}. (a) TGA thermograms; (b) DSC curves; (c) X-ray diffractograms.

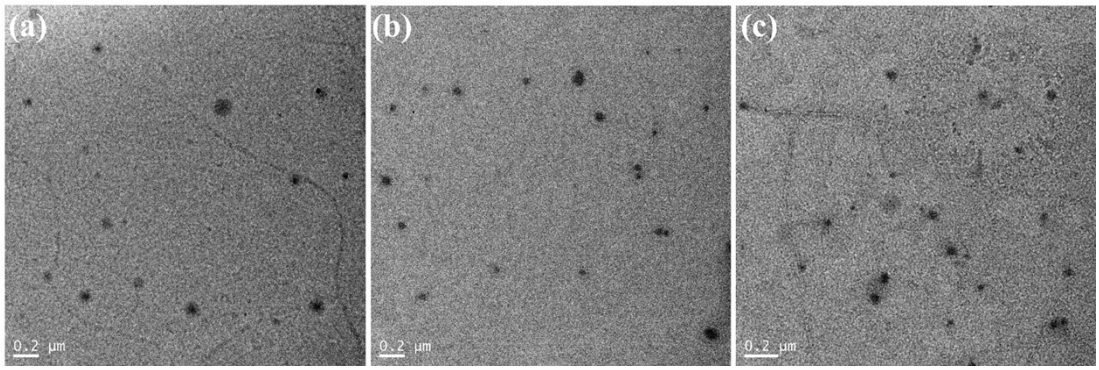

Fig. S6 TEM images of $PHEAA_{100}$-*g*-PCL_{20} synthesized by three methods. (a) RAFT/ROP binary polymerization; (b) "grafting-through; (c) "grafting-from".

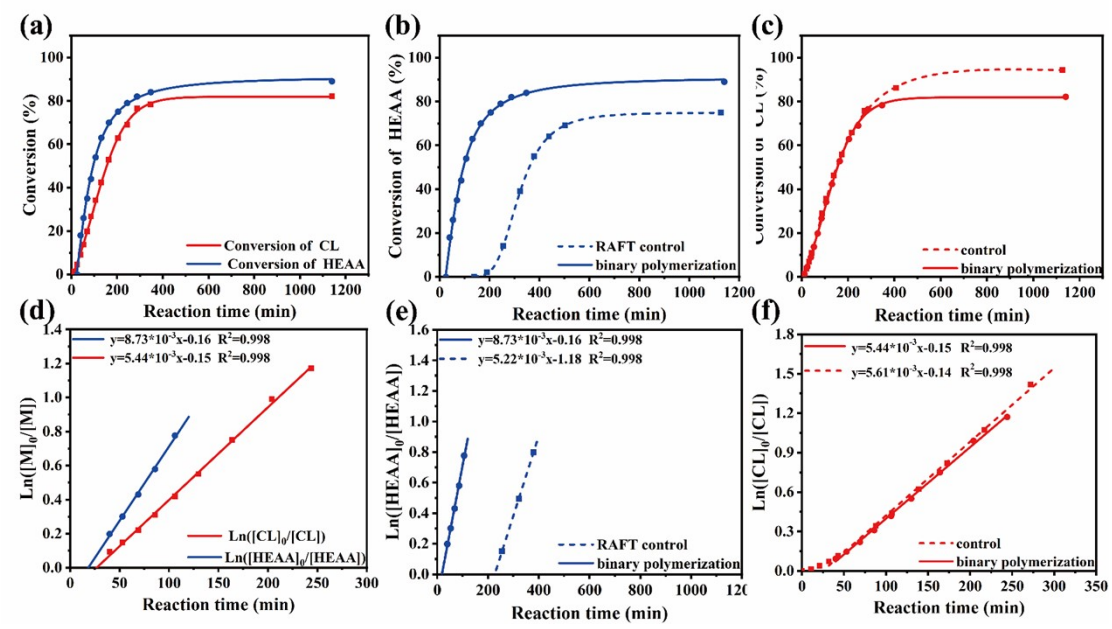

Fig. S7 Kinetic curves of $PHEAA_{100}$-*g*-PCL_{20} synthesized by RAFT/ROP binary polymerization and corresponding kinetics of RAFT control and ROP control. (a) Conversion of HEAA (blue solid line) and ε-CL (red solid line) versus reaction time in binary polymerization; (b) Conversion of HEAA versus reaction time in binary polymerization (blue solid line) and in RAFT control (blue dashed line); (c) Conversion of ε-CL versus reaction time in binary polymerization (red solid line) and in ROP control (red dashed line); (d) $Ln([M]_0/[M])$ of HEAA (blue solid line) and ε-CL (red solid line) versus reaction time in binary polymerization; (e) $Ln([M]_0/[M])$ of HEAA versus reaction time in binary polymerization (blue solid line) and in RAFT control (blue dashed line); (f) $Ln([M]_0/[M])$ of ε-CL versus reaction time in binary polymerization (red solid line) and in ROP control (red dashed line).

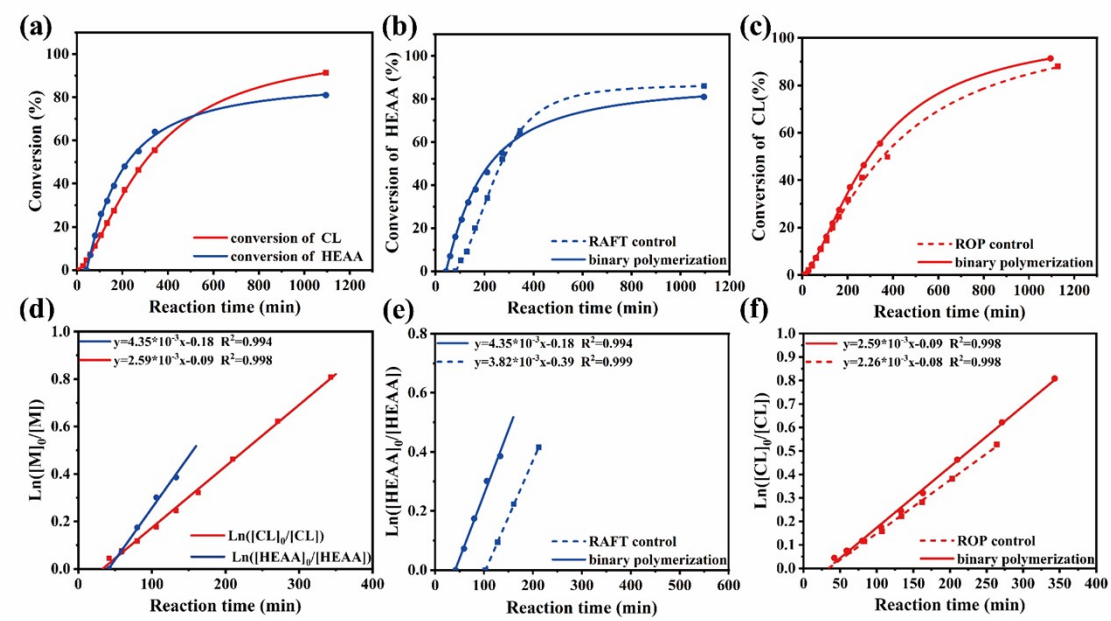

Fig. S8 Kinetic curves of PHEAA$_{50}$-*g*-PCL$_{40}$ synthesized by RAFT/ROP binary polymerization and corresponding kinetics of RAFT control and ROP control. (a) Conversion of HEAA (blue solid line) and ε-CL (red solid line) versus reaction time in binary polymerization; (b) Conversion of HEAA versus reaction time in binary polymerization (blue solid line) and in RAFT control (blue dashed line); (c) Conversion of ε-CL versus reaction time in binary polymerization (red solid line) and in ROP control (red dashed line); (d) Ln([M]$_0$/[M]) of HEAA (blue solid line) and ε-CL (red solid line) versus reaction time in binary polymerization; (e) Ln([M]$_0$/[M]) of HEAA versus reaction time in binary polymerization (blue solid line) and in RAFT control (blue dashed line); (f) Ln([M]$_0$/[M]) of ε-CL versus reaction time in binary polymerization (red solid line) and in ROP control (red dashed line).

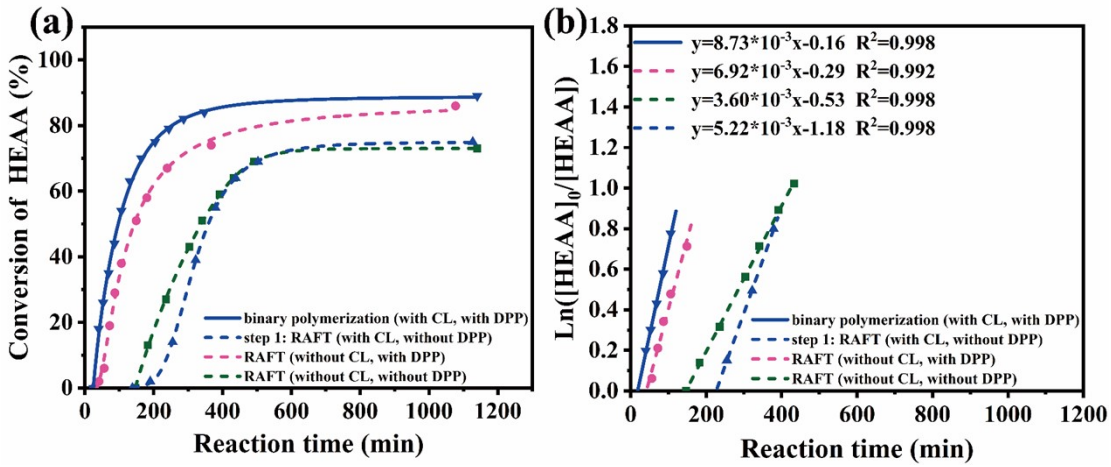

Fig. S9 Kinetic curves of RAFT polymerization at different reaction conditions. (a) Conversion of HEAA versus reaction time; (b) Ln([M]$_0$/[M]) of HEAA versus reaction time

Construction of RAFT/ROP binary polymerization kinetic model

In the RAFT/ROP binary polymerization, the hybrid function Φ_i (i = 1, 2; 1 denotes HEAA, 2 denotes ε-CL) was incorporated into the kinetic equation to represent the relationship between RAFT and ROP. The kinetic model could be described using the following equation:

$$\frac{dM_1}{dt} = -k_{11} \cdot M_1^{\alpha_1} \cdot \Phi_1 \qquad \Phi_1 = e^{-\varphi_{21} \cdot p_2^m} \tag{1}$$

$$\frac{dM_2}{dt} = -k_{22} \cdot M_2^{\alpha_2} \cdot \Phi_2 \qquad \Phi_2 = e^{-\varphi_{12} \cdot p_1^n} \tag{2}$$

where (1) represents the rate of consumption of the HEAA, while (2) represents the rate of consumption of the ε-CL. M_1 refers to the concentration of HEAA, and M_2 refers to the concentration of ε-CL. The p_1 represents the conversion of HEAA, and the p_2 represents the conversion of ε-CL. k_{11} represents the RAFT homopolymerization rate constant, while k_{22} represents the ROP homopolymerization rate constant. Since both RAFT and ROP exhibited first-order kinetic behavior, we assigned $\alpha_1 = \alpha_2 = 1$. Therefore, the kinetic model could be further described by the following equation:

$$\frac{dM_1}{dt} = -k_{11} \cdot M_1 \cdot \Phi_1 \qquad \Phi_1 = e^{-\varphi_{21} \cdot p_2^m} \tag{3}$$

$$\frac{dM_2}{dt} = -k_{22} \cdot M_2 \cdot \Phi_2 \qquad \Phi_2 = e^{-\varphi_{12} \cdot p_1^n} \tag{4}$$

In order to optimize the kinetic model, the values of m and n in the hybrid function Φ were discussed. Specifically, this discussion focuses on the cases where m and n were equal to 0, 1, and 2. Three graft copolymers with varied DPs of backbone and side chains were fitted as shown in the Fig. S10-S12.

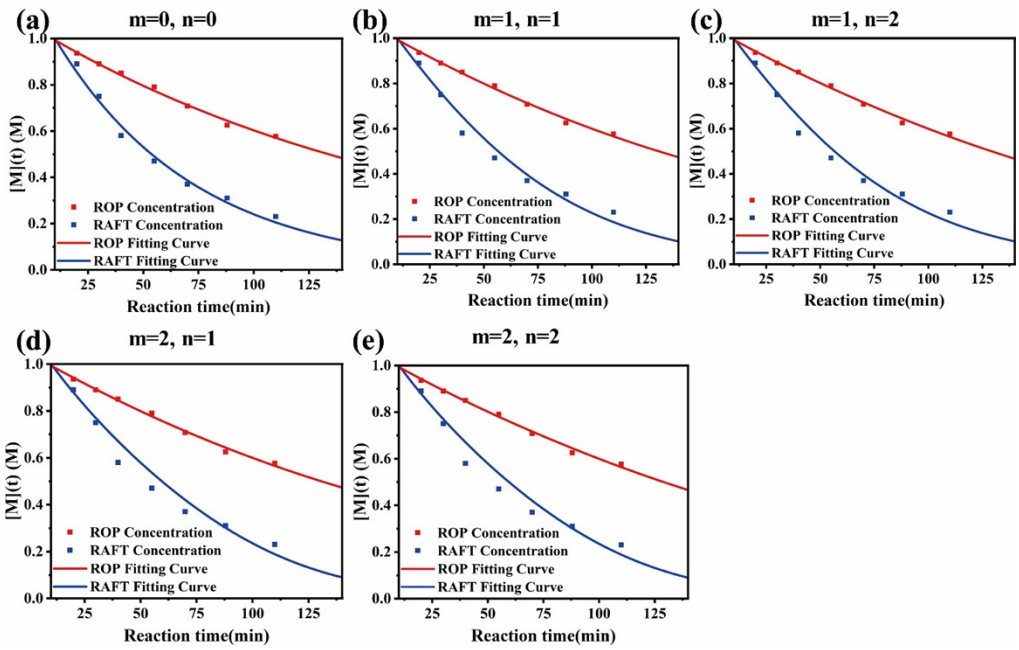

Fig. S10 Simulation of RAFT/ROP binary polymerization for different m, n values in $PHEAA_{50}$-*g*-PCL_{20} (dots for experimental results, lines for simulation results; red for ROP, blue for RAFT polymerization).

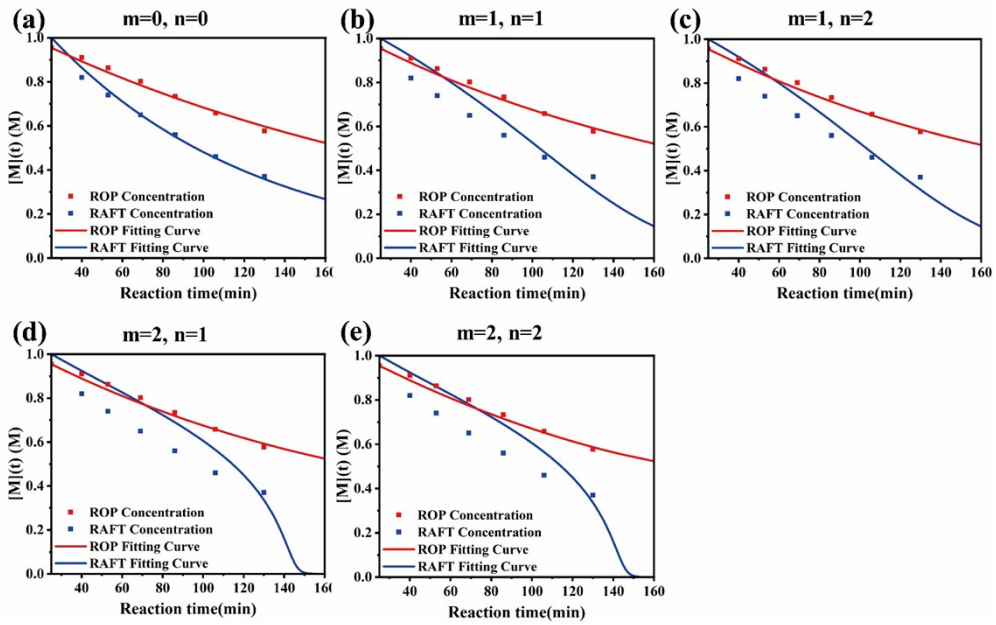

Fig. S11 Simulation of RAFT/ROP binary polymerization for different m, n values in $PHEAA_{100}$-*g*-PCL_{20} (dots for experimental results, lines for simulation results; red for ROP, blue for RAFT polymerization).

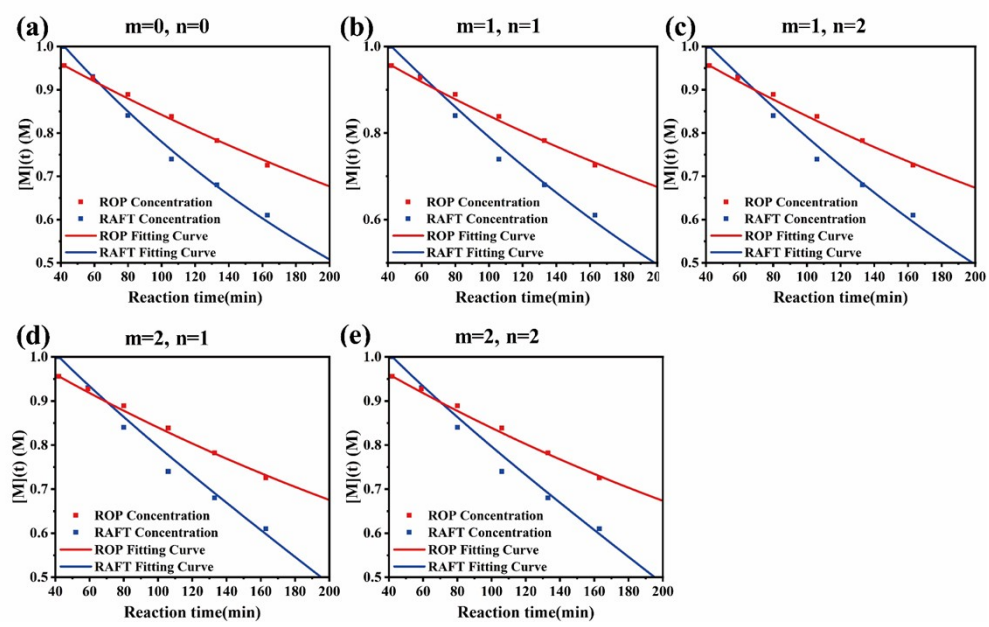

Fig. S12 Simulation of RAFT/ROP binary polymerization for different m, n values in $PHEAA_{50}$-*g*-PCL_{40} (dots for experimental results, lines for simulation results; red for ROP, blue for RAFT polymerization).

The figures illustrate that when both m and n were equal to 0, the fitted curves aligned closely with the experimental data for kinetic process, as different values were assigned to m and n, the fitted curves started to deviate to varying extents. Hence, the hybrid function was ultimately chosen to be m = n = 0, leading to the determination of the RAFT/ROP binary polymerization kinetic model described in equations (5) and (6):

$$\frac{\mathrm{d}M_{\mathrm{RAFT}}}{\mathrm{d}t} = -k_{\mathrm{RAFT}} \cdot M_{\mathrm{RAFT}} \cdot e^{-\varphi_{\mathrm{ROP/RAFT}}} \tag{5}$$

$$\frac{\mathrm{d}M_{\mathrm{ROP}}}{\mathrm{d}t} = -k_{\mathrm{ROP}} \cdot M_{\mathrm{ROP}} \cdot e^{-\varphi_{\mathrm{RAFT/ROP}}} \tag{6}$$